Entropy-Based Local Irregularity Detection for High-Speed Railway Catenaries With Frequent Inspections

Hongrui Wang, *Student Member, IEEE*, Zhigang Liu, *Senior Member, IEEE*, Alfredo Núñez, *Senior Member, IEEE*, and Rolf Dollevoet

***Abstract*— The condition-based maintenance of high-speed railway catenary is an important task to ensure the continuous availability of train power supply. To improve the condition monitoring of catenary, this paper presents a novel scheme to detect catenary local irregularities using pantograph head acceleration measurements. First, a series of experimental inspections is carried out in a section of the Beijing–Guangzhou high-speed line in China. The time intervals between the inspections are shortened from the traditional six months to about 40 days, which enables monitoring the short-term degradation of local irregularities. Then, based on the wavelet packet entropy, an approach is proposed to detect local irregularities with different scales in length. Criteria for identifying and verifying the local irregularities are established based on the gradient and repeatability of entropy from multiple measurements. Results from the experimental inspections show that different scales of local irregularities can be detected by the proposed scheme. By using frequent inspections, local irregularities can be effectively verified after about seven inspections. The spatial distribution of local irregularities is found to be closely related to the catenary structure. These findings provide valuable information to deploy the scheme for a railway network.**

***Index Terms*— Catenary condition monitoring, high-speed railway, inspection interval, local irregularity, wavelet packet entropy.**

I. Introduction

THERE are currently over 30 000 km of high-speed railway lines worldwide. Most of the high-speed trains are powered by electricity transmitted from the catenary suspended above the rail. Fig. 1 shows the basic components of catenary in one span between two masts, including the messenger wire, contact wire, and dropper. Both ends of the messenger and contact wires in several adjacent spans (an anchoring section) are anchored to keep certain tensions in the wires. The pantograph mounted on the train roof collects electric current when slides through the contact wire. Generally, the contact wire height along the entire line must maintain a good consistency and regularity to ensure the current collection quality. For railway infrastructure management, the irregularity of contact wire is a major issue [1]–[3]. Contact wire irregularities are unfavorable deviations in the contact wire height (as shown by the dashed lines in Fig. 1) and thickness, which can affect the dynamic contact with a pantograph in the vertical direction. Because a local irregularity can induce a transient impact when a pantograph passes through, it normally has a short deterioration period and high impact on the catenary condition that can impair the life cycle of catenaries [4], [5]. Thus, local irregularities of contact wire should be timely detected to prevent severe damages to the catenary and pantograph. Due to this particularity, complete or partial wire replacement is usually the only maintenance option in the case of damaged or broken contact wires, which costs much time and money, and, sometimes, interrupts train services.

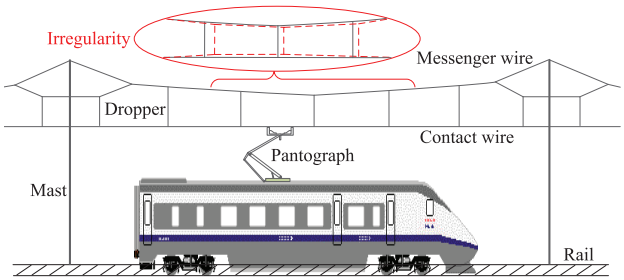

Fig. 1. Schematics of railway catenary and the irregularity of contact wire (dashed lines).

Condition monitoring is commonly adopted to facilitate the maintenance of catenary [6]. Previous studies developed approaches that vary with the employed measurements to assess the catenary condition based on periodical inspections. The pantograph–catenary contact force (PCCF) is the preferred parameter to measure theoretically [7], [8], since the interaction between catenary and pantograph can be directly reflected by the contact force. However, the general

Manuscript received June 23, 2018; revised September 1, 2018; accepted November 3, 2018. Date of publication December 4, 2018; date of current version September 13, 2019. This work was supported in part by the National Natural Science Foundation of China under Grant U1434203 and Grant U1734202, in part by the Sichuan Province Youth Science and Technology Innovation Team under Grant 2016TD0012, and in part by the China Railway Corporation Science and Technology Research and Development Program under Grant 2015J008-A. The Associate Editor coordinating the review process was Datong Liu. *(Corresponding author: Zhigang Liu.)*

H. Wang is with the School of Electrical Engineering, Southwest Jiaotong University, Chengdu 610031, China, and also with the Section of Railway Engineering, Delft University of Technology, 2628CN Delft, The Netherlands (e-mail: soul_wang0@163.com).

Z. Liu is with the School of Electrical Engineering, Southwest Jiaotong University, Chengdu 610031, China (e-mail: liuzg_cd@126.com).

A. Núñez and R. Dollevoet are with the Section of Railway Engineering, Delft University of Technology, 2628CN Delft, The Netherlands (e-mail: a.a.nunezvicencio@tudelft.nl; r.p.b.j.dollevoet@tudelft.nl).

Color versions of one or more of the figures in this article are available online at http://ieeexplore.ieee.org.

Digital Object Identifier 10.1109/TIM.2018.2881529

requirement for the PCCF measurement [9], in terms of sensor placement, accuracy, validation, and so on, is high and expensive to implement. Optionally, the displacement or acceleration of the pantograph, the contact wire, or the contact point can be employed as substitutes [10]. These parameters can be directly measured by displacement and acceleration sensors [11], or indirectly calculated from high-resolution images [12], [13].

Using the aforementioned parameters, some key performance indicators (KPIs) can be computed and then compared with the predetermined thresholds for condition assessment. For detecting local irregularities of contact wire specifically, both PCCF and pantograph head (pan-head) acceleration have been employed to establish KPIs. The statistical distribution and kurtosis of PCCF [2] and the root mean square of pan-head acceleration [4] were used for detecting irregularities. Recently, KPIs based on the frequency or wavelength of measurement data have been gaining attention. Frequency-based KPIs can reveal the contact wire irregularities in an early stage before the time-domain KPIs could. The quadratic time–frequency representation of PCCF was found to be feasible for detecting contact wire irregularities [14]. But, the localization accuracy for detecting local irregularity was unsatisfactory. Because local irregularities have limited impact on the pantograph–catenary interaction compared with the intrinsic structural parameters of catenary, including the anchoring length, span length, and interdropper distance [15]–[17], they are, generally, not easy to identify from the PCCF or pan-head acceleration. To address this issue, extracting the frequency components attributed to the structural parameters can be a preprocessing step before obtaining KPIs [16].

After preprocessing, a KPI should be accordingly established for detecting the local irregularities. As introduced earlier, previously employed KPIs, such as kurtosis, root mean square, and time–frequency representation, can also be applied. However, two main properties make them unfavorable for large-scale applications in practice as follows.

1) *Lack of General Applicability:* These KPIs are developed to focus on certain types of irregularities, while the irregularities actually have different shapes and lengths that induce different responses due to various causes, such as wear, incorrect tension of wires, and so on.
2) *Implementations Are Not Simple Enough:* There are parameters to be predetermined for previous KPIs, such as the window length of analyzed data, resolution parameters for time–frequency representation, and so on. Also, the comparison of KPIs requires prior knowledge on the defect types and the corresponding vibration responses, so that irregularities can be correctly diagnosed.

To detect generic local irregularities using frequency-based KPIs, the indicative frequency range are not constant, because the length or wavelength of local irregularities varies from centimeter [5] to tens of meters [14] attributed to different causes. In such a case, determining the indicative frequencies becomes problematic, since the types and locations of local irregularities existing in a railway line are unknown and changing with time. Therefore, an integrated KPI is proposed in this paper to circumvent identifying the indicative frequency ranges and also simplify the detection procedure for practice.

Recent studies [5], [18] showed that the wavelet transform is effective for analyzing the local characteristics of pantograph–catenary interaction because of the well-proven superiority of wavelet transform for identifying singularity in signal processing [19]. This superiority is rooted in the wavelet basis function that can be scaled and translated in time, while methods, such as the Fourier transform and the Hilbert–Huang transform [20], are based on the functions with full scale in time. It has been widely used for detecting local features, such as rail defects [21], [22], electrocardiograph anomalies [23], and bearing faults [24]. Based on the component signals decomposed by the wavelet transform, a KPI is often extracted from a component signal (or the corresponding wavelet coefficients) with the indicative frequency range depending on the problem to be solved. To establish an integrated KPI in this paper, the information contained in all the component signals should be combined together. Thus, the concept of entropy, which is a measure of order or disorder of a dynamic system, can be employed to establish the wavelet entropy [25] as the KPI. The local irregularities induce certain transient disorders in the pantograph–catenary dynamic interaction. Because the wavelet entropy is proven to reflect the degree of order or disorder associated with a multifrequency signal response [26], it is suitable for analyzing both the PCCF and pan-head acceleration.

Besides the difficulty from the signal processing perspective, another situation that is also not in favor of the local irregularity detection is the periodical inspection for catenaries. Currently, the inspections are carried out annually or semi-annually by a dedicated inspection train. However, the time interval between every inspection is too long to monitor the short-term degradation of defects [4]. The results from two successive inspections, when comparing with each other, cannot reflect adequately the evolvement of the catenary condition. For high-speed lines, especially lines with high traffic densities, a shorter inspecting period certainly will benefit the detection and prediction of defects causing local irregularities, so that infrastructure managers can control further damages and reduce potential safety threats. Nevertheless, this is on condition that the data measurements and analyses can be timely arranged and implemented.

In this context, a series of experimental inspections was performed on a section of the Beijing–Guangzhou high-speed railway in China, which has an annual passenger demand of over 100 million. The inspections are carried out with a time interval shorter than two months. In this way, the potential to improve the stability and safety of high-speed catenary by timely eliminating or mitigating local irregularities can be explored. Moreover, instead of running at a low speed, the inspections are deliberately carried out at or close to the commercial speed of the railway line. It imitates the operation of commercial trains to examine if future inspections could be performed by commercial trains so that overnight inspections that are costly and sometimes interfere with a regular operation can be circumvented. Also, multiple commercial trains mounted with a measurement system can substantially

shorten the inspection interval to cover the entire railway line or network, which is more feasible and economical compared with manufacturing and operating a number of specialized inspection trains.

Using the data measured from the aforementioned experimental inspections, this paper employs the pan-head acceleration as the source of KPI to detect local irregularities in high-speed railway catenaries. In a previous study [27], the motivation, feasibility, and preliminary processing technique of using the pan-head acceleration to reduce the system cost and technical difficulty of catenary condition monitoring is presented. This paper extends those ideas into application and further proposes an approach for catenary local irregularity detection. The rest of this paper is organized as follows. The data set and data processing techniques employed in the proposed approach are introduced in Section II. Section III presents an approach for detecting local irregularities with different scales in length. Section IV presents and discusses the detection results obtained from the experimental inspections. Some conclusions and outlooks are given in Section V toward the implementation of the detection scheme for a network of railway lines.

II. Data Description, Preprocessing, and Wavelet Packet Entropy

This section first describes the measurement data that are required for the proposed approach, using the data set measured from the experimental inspections as an example. Then, a preprocessing procedure is proposed to extract the essential frequency components contained in pan-head accelerations. Finally, the wavelet packet entropy is introduced for the preprocessed accelerations, which provides KPIs to identify and verify local irregularities later in Section III.

A. Data Description

As an input for the proposed approach, a dedicated inspection or commercial train installed with a pantograph–catenary monitoring system is required. The system should measure parameters concerning the condition of catenary, which are the pan-head acceleration and the height and stagger of contact wire for this approach. Also, a more frequent inspection strategy compared with the previous inspection interval of half a year should be employed. The new interval is preferably less than three months.

In the case of the aforementioned experimental inspections, an integrated on-board measurement system was employed to measure the pan-head vertical acceleration and the height and stagger of the contact wire. Simultaneously, the speed and location of the inspection train and the passage of masts between spans are also recorded. The measurements comply with the technical specification enacted by the China Railway Corporation in 2012 [28], in which requirements on the inspection of catenary and pantograph–catenary interaction are put forward. Table I presents the measurement range and accuracy required for the measured parameters. An example of the measured data set is shown in Fig. 2. The sampling rate for all measurements is a fixed spatial interval of 0.25 m.

TABLE I
Technical Specifications for the Parameters Measured [28]

Parameter	Measurement range	Accuracy
Pan-head acceleration	0g–100g	1g
Contact wire height	5000 mm–7000 mm	25 mm
Contact wire stagger	−600 mm–600 mm	25 mm
Train speed	0 km/h–500 km/h	0.1 km/h

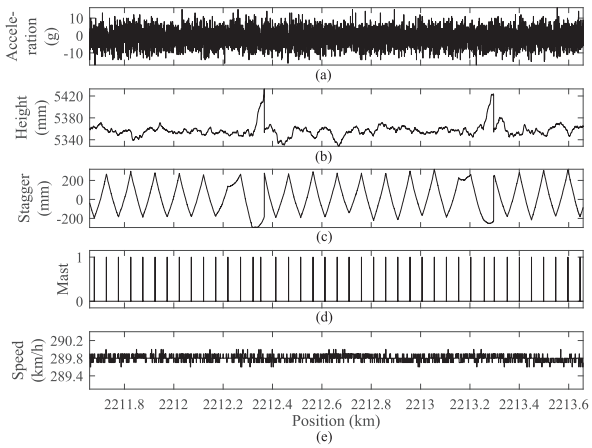

Fig. 2. Set of inspection data. (a) Pan-head vertical acceleration. (b) Contact wire height. (c) Contact wire stagger. (d) Mast passage. (e) Train speed.

Fig. 2(a) shows the vertical acceleration of pan-head in the unit of the gravitational acceleration $g \approx 9.81\ \mathrm{ms}^{-2}$. Fig. 2(b) and (c) shows the height and stagger of contact wire, respectively. It can be seen that there are two locations with abnormal variations of value at around 2212.4 and 2213.3 km in the contact wire height and stagger. These types of variation appeared because the inspection train was passing through the overlapping section between two anchoring sections of the catenary. In Fig. 2(d), the indicator of mast passage is shown as a Boolean variable with 1 and 0 denoting the occurrence and the absence of a mast, respectively. During the measurements, the speed of the inspection train was maintained to be approximately constant around 289.8 km/h, as shown in Fig. 2(e). The measurements other than the pan-head acceleration are considered as auxiliaries to support the outcomes from acceleration.

B. Preprocessing

The pan-head acceleration signal contains essential frequency components, namely the catenary structure wavelengths (CSWs) caused by the cyclic structure of catenary [16]. As has been explained in [27], the identification of the CSWs in pan-head acceleration can be realized based on the ensemble empirical mode decomposition (EEMD) [29]. It can adaptively sift out the CSW regardless of variations in the catenary structure, operation speed, and pantograph type. Given an acceleration signal $x(t)$, the EEMD first decomposes the signal into several intrinsic mode functions (IMFs) $d_l j(t)$, $l = 1, 2, \ldots, N$ and a residual $r(t)$ that satisfy

$$x(t) = \sum_{l=1}^{N} d_l(t) + r(t). \tag{1}$$

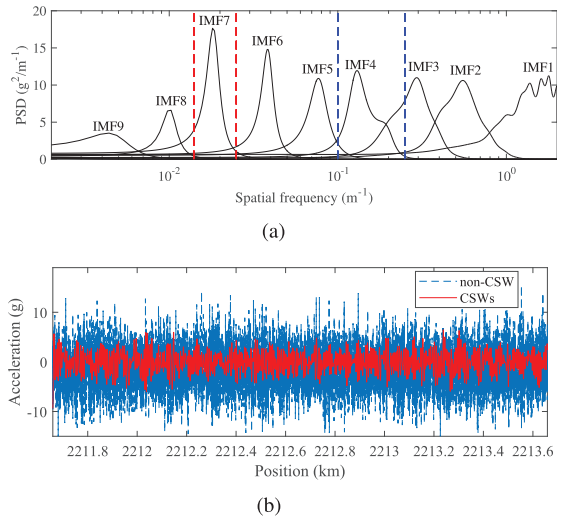

Fig. 3. (a) PSDs of the IMFs and (b) corresponding CSWs and non-CSW signal.

In [27], the identification of CSWs is realized by eliminating IMFs with frequencies higher than the frequency range of CSWs, based on the power spectrum densities (PSDs) of the IMFs. To further explore the usage of acceleration signal, this paper utilizes both the CSWs part and non-CSW part of the signal. Concretely, because the CSWs normally range between certain intervals of spatial frequency, the CSWs contained in the original acceleration signal can be separated from the non-CSW signal. This can be done by PSDs of the IMFs with a Boolean variable

$$\Delta_l = \arg\max_f [P_l(f)] \langle f_1 \wedge \arg\max_f [P_j(f)] \rangle f_2 \tag{2}$$

where $P_l(f)$ is the PSD of lth IMF $d_l(t)$, $\arg\max_f [P_l(f)]$ denotes the argument of the maximum $P_l(f)$, and f_1 and f_2 are the upper and lower frequency boundaries to identify if an IMF is a CSW, respectively. The common pairs of value for the frequency boundaries are (0.014 m^{-1}, 0.025 m^{-1}) and (0.1 m^{-1}, 0.25 m^{-1}), corresponding to the interdropper distance wavelength and the span wavelength, respectively, according to [16]. Using the two pairs of frequency boundary, the CSWs $x_c(t)$ can be obtained by summing the identified IMFs, while the non-CSW residual $x_n(t)$ is the sum of the rest of IMFs and the residual $r(t)$. The two signals satisfy

$$x(t) = x_c(t) + x_n(t). \tag{3}$$

Thus, the acceleration signal is essentially decomposed into two signals that are the CSWs and the non-CSW signal after the preprocessing. For example, PSDs of the IMFs decomposed from the acceleration signal in Fig. 2 are shown in Fig. 3(a). Based on (2), the IMFs whose peak of PSD falls within the frequency intervals indicated by the red and blue dashed lines, namely the 4th and 7th IMFs, are identified as CSWs. As a result, the CSWs and the non-CSW signal of the original acceleration signal are reconstructed, as shown in Fig. 3(b). Generally, the original signal should not be segmented beforehand to preserve intact the information contained in both the reconstructed signals. This also helps to avoid the influence of the end effect of EEMD [29] by minimizing the number of signal ends.

C. Wavelet Packet Entropy for CSWs and Non-CSW Signal

The pan-head acceleration is decomposed into two signals, namely the CSWs and the non-CSW signal, after the preprocessing. The CSWs can be regarded as the component resulting from the stiffness variation of contact wire in cycles of span and interdropper distance. Thus, defects with the length or wavelength that is equal or close to span and interdropper distance can be reflected in the CSWs. Meanwhile, other defects that induce different frequency responses are reflected in the non-CSW signal. For both the signals, the wavelet packet transform (WPT) [30] is employed for a comprehensive feature extraction. Concretely, taking the CSWs $x_c(t)$ as an example, it can be decomposed into 2^j component signals after j ($j \in \mathbf{N}$) levels of WPT as follows:

$$x_c(t) = \sum_i^{2^j} x_j^i(t). \tag{4}$$

Each component signal $x_j^i(t)$ can be expressed as

$$x_j^i(t) = \sum_{k=-\infty}^{\infty} c_{j,\varphi}^i \psi_{j,\varphi}^i(t) \tag{5}$$

where $\psi_{j,\varphi}^i(t)$ is a wavelet packet function and integers i, j, and φ are the modulation, scale, and translation parameters, respectively. The wavelet packet coefficients $c_{j,\varphi}^i$ are obtained from

$$c_{j,\varphi}^i = \int_{-\infty}^{\infty} x_c(t) \psi_{j,\varphi}^i(t) dt. \tag{6}$$

Compared with the conventional wavelet transform that only decomposes the low-frequency component of a given signal after the first level, the WPT decomposes signals completely at every level that results in higher resolution in the high-frequency band. This ensures the extraction of high-frequency features that can be attributed to local or short-wavelength excitations, which is important for identifying local defects.

However, the complete decomposition of WPT may excessively divide the frequency band of the original signal into narrow frequency bands. Concretely, a component signal at a low level that contains useful information for irregularity detection can be unfavorably decomposed into two component signals that are lack of physical meanings. This can lead to inaccurate KPIs for further application. To address this issue, a common solution is to find the optimal decomposition tree for the given signal based on the entropy of nodes [31]. Starting from the root node of the full WPT tree, the employed entropy-based criterion computes and compares the entropy of every parent node and the two nodes split from it. To obtain the optimal tree, a parent node is split only if the sum of the entropy of the two nodes is lower than the entropy of itself. In this way, the given signal has the lowest information cost with WPT based on the optimal tree. Taking the CSWs and the non-CSW signal shown in Fig. 3(b) as examples,

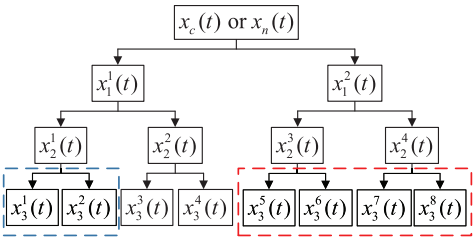

Fig. 4. Optimal trees determined for the WPT of the CSWs $x_c(t)$ and the non-CSW signal $x_n(t)$. The red and blue dashed lines indicate nodes that are discarded by the entropy-based criterion for $x_c(t)$ and $x_n(t)$, respectively.

TABLE II
TYPICAL CATENARY DEFECTS AND THE RESULTING SCALES OF LOCAL IRREGULARITIES

Defect type	Scale
Incorrect tension of catenary	Spans
Unrecovered thermal expansion of catenary	Spans
Midpoint anchor misregulation	Tens of meters
Incorrect positioning of overlap	Meters
Inaccurate dropper length or position	Meters
Inaccurate steady arm angle	Meters
Uneven wear	Meters or Centimeters
Hard point	Centimeters

the optimal trees determined from the three-level WPT of both the signals are shown in Fig. 4. This is implemented by using the MATLAB toolbox in [32]. It can be seen that the optimal tree varies with the signals. This consequently changes the result of WPT from, for example, (4) to as follows:

$$x_c(t) = \sum_{\{i,j\}\in \mathbf{S_c}} x_j^i(t) \tag{7}$$

where $\mathbf{S_c}$ is the set of component signals remained in the optimal tree of the CSWs $x_c(t)$.

The component signals at the terminal nodes of the optimal tree contain specific frequency bands decomposed from the original signal. This enables feature extraction at the concerned frequency bands that are related to abnormal excitations. To obtain a KPI that characterizes the features for local irregularity detection, the Tsallis wavelet entropy is employed. The Tsallis entropy is a kind of entropy that measures the disorder of a system. Combining with the signal decomposition results from wavelet transform, it has been applied to the identification of short-duration or transient process in the response of faulty systems [33]–[35]. In this paper, it is employed as an indicator to integrate the results from WPT. For a set of probabilities $\{p_{i,j}\}$ with $\sum_{\{i,j\}\in\mathbf{S}} p_{i,j} = 1$, the general Tsallis entropy can be defined as

$$S = \frac{1}{q-1}\left(1 - \sum_{\{i,j\}\in\mathbf{S}} (p_{i,j})^q\right), \quad q \in \mathbf{R} \tag{8}$$

where q is the nonextensive parameter, and in the case of Tsallis wavelet entropy, $p_{i,j}$ is the relative wavelet packet energy of the ith node at the jth level computed by

$$p_{i,j} = \frac{E_{i,j}}{\sum_{\{i,j\}\in\mathbf{S}} E_{i,j}} \tag{9}$$

where $E_{i,j}$ is the wavelet packet energy for the ith node at the jth level. For a discrete signal, the computation of $E_{i,j}$ should be done within a time window centered around an arbitrary time instant t_n with

$$E_{i,j}(t_n) = \sum_{t\in T_n} \left(x_j^i(t)\right)^2 \tag{10}$$

where the time window $T_n = \{t : |t - t_n| \le (L_w/2)\}$ denotes the set of time instants contained in the window length L_w. This window length determines the length of data on which the Tsallis wavelet entropy is based. It can shift and scale in the time domain in a way serving as a flexible detector for anomaly detection at a different scale and location. Thus, the selection of window length becomes crucial for the local irregularity detection as will be presented in Section III.

III. LOCAL IRREGULARITY DETECTION

The term "local" is a relative description of irregularity that depends on the total contact wire length corresponding to the data scale. For instance, for the data measured from kilometers of contact wire, the contact wire irregularity with a length of hundreds of meters can thus be regarded as a local one. It means that the local irregularity only occupies a small portion of the total length of the contact wire concerned. In this context, the selection of data length to be analyzed becomes crucial for local irregularity detection. It determines the length of local irregularity that can be reflected by the data. Table II shows several types of typical catenary defect that can lead to different scales of local irregularity. For a long data series from a continuous measurement, the window length selected for local irregularity detection should be varying instead of being fixed, so that different types of local irregularity can be reliably identified. It is also beneficial for recognizing the cause of local irregularities due to the enhanced local information. Therefore, this section presents a varying window strategy for local irregularity detection.

A. Entropy Computation With Varying Windows

As presented in (10), the wavelet packet energy $E_{i,j}(t_n)$ computed in the window length L_w decides on which data scale, the Tsallis wavelet entropy in (8), is based. The idea is to employ different window lengths concerning the scales of defects given in Table II. It can be seen that the scale of local irregularities varies from hundreds of meters (spans) to centimeters. To determine the precise window length to be employed, the actual variation of the catenary structural parameter is taken into consideration for two main reasons as follows.

1) The scales of local irregularities are all associated with physical causes that are inaccurate structure configuration or damages attributed to pantograph–catenary interaction. Because the structural parameters of catenary affecting the formation of local irregularities are not strictly consistent along the entire line, these parameter variations should be considered for window length selection.

TABLE III
THREE PAIRS OF SCALE FOR ENTROPY COMPUTATION

Scale	Window length $L_w(t_n)$	Time instant t_n
1	Lengths of anchoring sections	Positions of masts
2	Lengths of spans	Every 5 m
3	5 m	Every 0.25 m

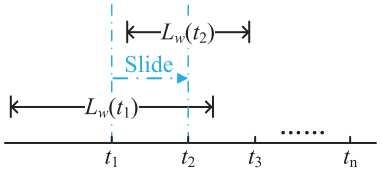

Fig. 5. Illustration of the varying window with length $L_w(t_n)$ sliding through time instants t_n.

2) Assuming that a fixed window length $L_w = 300$ m, which equals to about six spans, is employed as the window for the scale of spans. When this fixed window slides through the data series measured from a catenary with uneven span lengths, it will cover a different combination of spans with both ends of the window shifting erratically in the middle of certain spans. This makes the resulting entropies less comparable with each other since they are based on the vibration responses of pantograph sliding through different local parts of the catenary. Therefore, it is preferred to not only use the varying window to detect local irregularities with different scales but also have windows that are adapted to the variation of the catenary structural parameter.

Making use of auxiliary measurements, the lengths of every anchoring section, the lengths of every span, and an average interdropper distance of 5 m in the catenary are employed as the varying window lengths. First, the distance between two adjacent overlapping sections, which can be obtained based on the contact wire height, is regarded as the length of an anchoring section. Using this window length, defects that have a scale of spans such as shown in Table II could be identified. Second, the distances between two adjacent masts indicated by the Boolean values of masts are regarded as the lengths of spans. Similarly, this window length helps to identify defects that have a scale within one span but longer than 5 m such as shown in Table II. Finally, the shortest window of 5 m is used to identify other defects with a scale shorter than 5 m, which are mostly wear and hard points in the contact wire. As concretely given in Table III, there are two key parameters in (10) involved in the varying window strategy. The first one is the window length L_w for entropy computation. The second one is the time instant t_n that decides where the midpoint of the window is located. As schematically shown in Fig. 5, the varying window slides through the signal as the time instant t_n increases in the time domain.

To pair with the aforementioned three scales of window length, three sets of time instant t_n are proposed accordingly. Basically, at each scale, the interval between adjacent time instants should not be longer than half of the window length, so that the full signal length can be entirely covered by the sliding window. This can be done by using the window lengths from the next scale as the intervals between time instants. As given in Table III, for Scale 1, the window lengths are the actual lengths of anchoring sections. The corresponding time instants are the positions of masts within every anchoring section, which makes the interval between two adjacent time instants equal to the window length of Scale 2 that is the length of span. Similarly, the time instants of Scale 2 correspond to the window length of Scale 3. Finally, for the shortest window length of Scale 3, the sampling interval of 0.25 m is employed to essentially compute the entropy at every sampling point. In this way, the entropy-based feature extractions can be performed at three scales corresponding to the lengths of the anchoring section, span, and interdropper distance in descending order. It can not only ensure the complete feature extraction at every scale but also avoid the extraction of redundant features among different scales. Most importantly, the computed entropy can be associated with certain physical meaning rooting in its spatial position and specific window length.

As introduced in Section II, for subsequent entropy computation, there are two signals, namely the CSWs and the non-CSW signal, decomposed by WPT with optimal trees. To apply the varying window strategy to both the signals, the physical meanings of both should be taken into consideration. The CSWs signal is, by definition, associated with the structural parameters of the catenary. It contains frequency components that are sensitive to the variation of span and interdropper distance along the catenary. This is in line with the effects of the varying window strategy at Scales 1 and 2, in which the window slides with the interval of span and interdropper distance, respectively, to detect anomalies in the frequency range related to the structural parameters. Thus, Scales 1 and 2 should be applied to the CSWs. For the same reason, the non-CSW signal is suitable to be processed by the Scale 3 varying window to detect anomalies at scales smaller than the main structural parameters. Based on the entropy computed at the three scales, the following presents the criteria for the identification and verification of local irregularities.

B. Local Irregularity Identification and Verification

In future inspections, if the pan-head acceleration is the sole source of indicator for catenary condition monitoring, it is crucial to establish the baseline and criterion for the diagnosis of acceleration signals. For dynamic measurements such as the pan-head acceleration, the data measured from a single inspection run is considered to be not so reliable in terms of repeatability under the interferences of measurement noise and environmental disturbance. This may lead to a false indication of defects or overlook of actual defects. With a shortened inspection interval, data from multiple runs can be used for cross-comparison to mitigate this effect and thus increase the hit rate, find new defects at an early stage, and obtain the degradation of different defects.

In practice, the signal baseline for the pan-head acceleration is normally measured from the acceptance test of the targeted pantograph–catenary system or early *in situ* inspections. It is

anticipated that the system performance will decline with the increase of service time so that infrastructure managers can keep track of the system condition by comparing new data with the baseline. For the experimental inspections in this paper, there is no historical reference, as it is a new attempt of the inspection strategy. Thus, the measurement data from the first inspection is regarded as the baseline for this particular case study. It should be noted that all data are measured from an existing line where the presence of local irregularities was expected, even for the first inspection performed among the nine inspections.

To identify the local irregularities that cause abnormal transients in the computed entropy, a criterion based on the variation of entropy is employed. For a series of entropy $S(t_n)$ computed by the varying window at any of the three scales, an abnormal transient could be an abrupt rise or fall in the entropy along the time. It can be mathematically described as the gradient of entropy defined as

$$G(t_n) = \frac{|S(t_{n+1}) - S(t_{n-1})|}{t_{n+1} - t_{n-1}}. \tag{11}$$

Then, to automatically identify and locate the abnormalities in a rather long entropy series computed from kilometers of data, the following criterion is employed:

$$Y(t_n) = \begin{cases} 1, & \text{if } |G(t_n)| > \mu + 3\sigma \\ 0, & \text{otherwise} \end{cases} \tag{12}$$

where μ and σ denote the mean and standard deviation (SD) of the entropy gradient $G(t_n)$, respectively. $Y(t_n)$ is a Boolean variable with value 1 and 0 denoting if the corresponding entropy value is abnormal or not, respectively.

Although this criterion decides the property of entropy in an absolute sense, it does not indicate necessarily the presence or absence of local irregularity. The identified abnormal entropy can be further verified by comparing with the baseline and historical results measured from the same location. The comparison must be carried out for entropies computed at the same scale. Taking the mth ($m > 1$) measurement in this paper as an example, its result at Scale k ($k \in \{1, 2, 3\}$) denoted by $Y_{m,k}(t_n)$ can be compared with the result of the earlier $(m-1)$th measurement at the same scale $Y_{m-1,k}(t_n)$ as follows:

$$Y_{m,(m-1),k}(t_n) = Y_{m,k}(t_n) \wedge Y_{m-1,k}(t_n) \tag{13}$$

where $Y_{m,(m-1),k}$ is the logical conjunction of $Y_{m,k}(t_n)$ and $Y_{m-1,k}(t_n)$. If $Y_{m,(m-1),k}(t_n)$ is 1 (true), it means that the results from the two inspections are consistent, since both the results are positive about the presence of local irregularity at the same location. If possible, this can be extended by tracing results back to the earliest inspection where the local irregularity first appeared, so the evolvement of irregularity can be observed. For the positive result that cannot find any trace of support from previous inspections, it can be temporarily labeled as a new potential local irregularity, which will be verified when subsequent inspections are performed. It should be noted that the result of a single inspection may generate several false positives and negatives. Thus, it is necessary to trace back more than one inspection when looking for support for a potential local irregularity. Generally, a potential local irregularity can be treated as a verified one when at least three positive results at the same location are successfully identified from the recent six inspections. This is to prevent the waste of maintenance resource on unverified defects. A generalized mathematical expression of the verification can be expressed as

$$Y_{\mathbf{M},k}(t_n) = Y_{m_1,k}(t_n) \wedge Y_{m_2,k}(t_n) \ldots \wedge Y_{m_q,k}(t_n) \tag{14}$$

where $m_1, m_2, \ldots, m_q \in \mathbf{M}$ and $\mathbf{M}$ is the set of measurement number selected for local irregularity verification with $(m_q - m_1) < 6$. For a potential local irregularity at t_n, it is verified only if $Y_{\mathbf{M},k}(t_n) = 1$ and the number of elements in $\mathbf{M}$ is no less than 3.

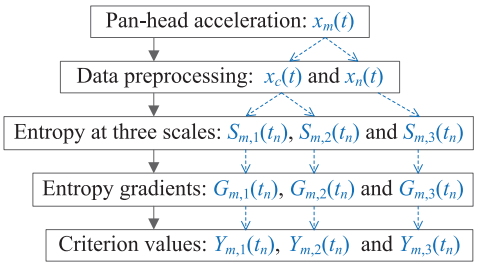

Fig. 6. Summarized process of the signal transformation in the proposed approach. The dashed lines with arrows indicate the relationships between the signals.

To sum up, Fig. 6 shows concisely the proposed approach with the transformation of the mth acceleration signal $x_m(t)$ to the Boolean variable $Y_{m,k}(t_n)$ at Scale k. The acceleration signal is first preprocessed and decomposed into the CSWs $x_c(t)$ and the non-CSW signal $x_n(t)$ by (3). At this point, the best trees of both the signals based on WPT are obtained, and the corresponding component signals at the terminal nodes are determined for entropy computations. Then, the entropy $S_{m,k}(t_n)$ at the three scales with varying windows is computed separately by (8). Accordingly, the entropy gradient $G_{m,k}(t_n)$ and the Boolean variable $Y_{m,k}(t_n)$ at the three scales are obtained. Finally, comparisons for verifying the local irregularities can be realized by (14). In theory, the proposed approach is simple to implement, because there is no parameter needing to be predetermined and tuned from the preprocessing step to the final verification. The entire process can be computed automatically as long as the input data meet the requirements. Also, the results are simplified to a single KPI that is the criterion value at three scales. This facilitates the maintenance decision-making when dealing with a massive amount of data from a railway network.

IV. Results and Discussion

The data set from the experimental inspections are employed to demonstrate the detection performance of the proposed approach. The inspections were carried out in a section of railway that is about 34.5 km long from the Beijing–Guangzhou high-speed line starting at 2211.6 km. As shown in Fig. 7, nine measurements are performed in the same section with an average interval of 39 days and the maximum less than 2 months. The time intervals are uneven in consideration of minimizing the impact on regular operation. During the nine measurements, a fixed train speed of 290 km/h is consistently

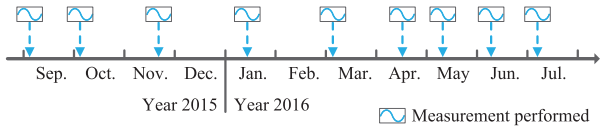

Fig. 7. Timeline of the experimental inspections.

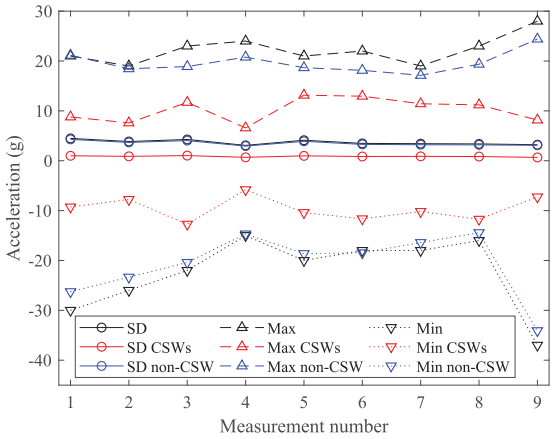

Fig. 8. Comparisons of the SD, maximum (Max), and minimum (Min) of the pan-head acceleration, the corresponding CSWs, and the non-CSW signal, respectively, from the nine measurements.

used, while the data measured during the acceleration and deceleration of the train are omitted. Although the environmental conditions such as the temperature and wind for the nine measurements were different due to the natural change of seasons, the measurement system is considered unaffected, because the system was designed to be functioning under the temperature from −40 °C to 70 °C in areas below 2500 m above sea level. Hereafter, the measurements are referred as measurement 1 to 9 in a chronological order.

Initially, it was difficult to discover any explicable pattern from the basic statistics of the nine acceleration data series. Fig. 8 shows the differences among the nine data series in terms of SD, maximum, and minimum, which reflect the degree of oscillation in the pan-head acceleration. The same statistics of the corresponding CSWs and the non-CSW signal are also shown. It can be seen that the SDs of the accelerations fluctuate slightly around 3.7 g for all the nine measurements. The corresponding SDs of the non-CSW signals in blue circles almost overlap with those of the accelerations with smaller values that fluctuate around 3.5 g. This similarity agrees with the case of contact force where, likewise, the SD of non-CSW signal fluctuates with the SD of force [16]. The maximum and minimum values of the accelerations and the non-CSW signals also show the same similarity. Meanwhile, the CSWs have smaller fluctuations with SDs at around 0.9 g and extrema changing with a different pattern compared with those of the accelerations and the non-CSW signals. In any case, it was not obvious that the acceleration is deteriorating with the increase of operational time. The same can be concluded from the PSDs of the accelerations shown in Fig. 9. It can be seen that the level of PSDs was neither growing nor declining

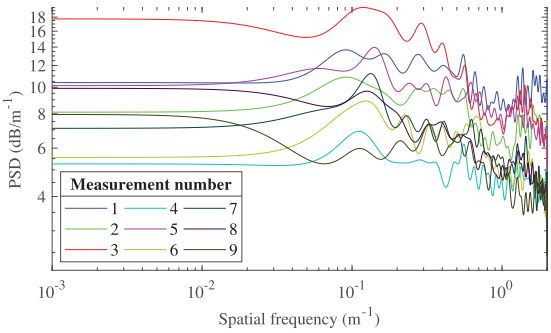

Fig. 9. Comparisons of the PSD of pan-head acceleration from the nine measurements.

consistently with the increase of measurement number. For example, measurements 3 and 4 were performed under similar speed. However, the PSD of acceleration from measurement 3 has the highest level of spectrum density, while the one from measurement 4 has the lowest.

Besides the randomness of pantograph vibration during the nine measurements, part of the reason for these uncertain results is that the indicators are globally computed from the entire data series. This can be improved by using local windows to examine the indicators of local data segments. The proposed approach is precisely this type of methodology, but with frequency indicators that help to identify early-stage irregularities which are hard to detect based on the time-domain statistics. The following demonstrates the detection results at the defined three scales separately and together.

A. Results at Each Scale

1) Scale 1: The first scale aims to detect local irregularity with respect to the length of anchoring sections based on the extracted CSWs. The irregularity at this scale indicates that the overall level of contact wire height or elasticity is abnormal, likely due to the incorrect tension or unrecovered thermal expansion of catenary wires. Fig. 10(a) shows the entropies computed at Scale 1. It can be seen that each entropy series fluctuates moderately with several notable peaks and troughs as the pantograph runs forward in position. Since the entropies were based on CSWs and window lengths at Scale 1, the fluctuation could be attributed mostly to the changes of the geographic condition along the line and differences in the catenary structure in order to adapt those changes. The entropy gradients shown in Fig. 10(b) provide more information on the degree of entropy fluctuations. It becomes relatively clear where the drastic changes happened in the entropies of CSWs. Based on the criterion defined in (12), the potential irregularities at Scale 1 from the nine measurements were identified and shown as red dots on the dashed threshold lines. Some locations of the potential irregularities from different measurements were overlapping with each other. According to the principle for local irregularity verification defined with (14), the locations of verified local irregularities based on all nine measurements are shown in Fig. 11. Four locations with irregularities are verified at Scale 1 because they were identified in at least three out of the nine measurements.

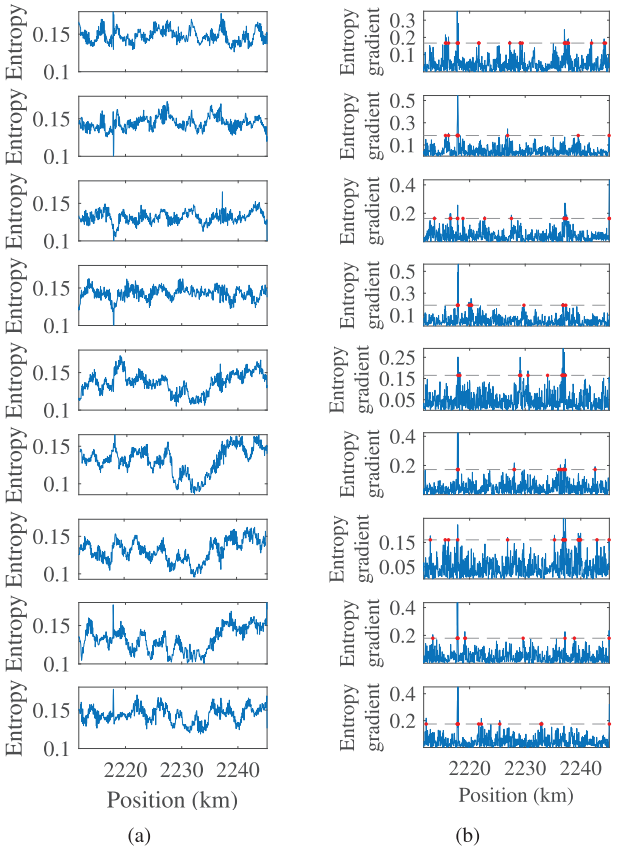

Fig. 10. (a) Entropies of the accelerations from measurement 1 to 9 (from top to bottom) at Scale 1. (b) Corresponding entropy gradients. The dashed lines depict the thresholds in (12) with red dots marking the gradients higher than the thresholds.

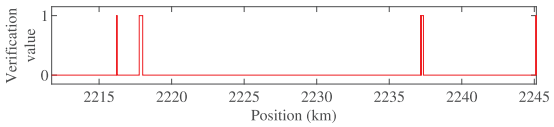

Fig. 11. Verified local irregularities at Scale 1 based on the nine measurements.

TABLE IV
NUMBERS OF THE MEASUREMENTS THAT VERIFY THE FOUR LOCAL IRREGULARITIES

Local irregularity	Position (km)	Measurement numbers
1	2216.2	1, 2, 3 and 7
2	2217.8	1, 2, 5, 6, 8 and 9
3	2237.2	1, 3, 6, 7 and 8
4	2245.0	2, 3, 7 and 8

To further investigate the results, Table IV provides the measurements from which the four local irregularities were identified. By referring to the inspection schedule shown in Fig. 7, it can be inferred that these measurements performed with short intervals are indeed necessary to enable the irregularity detection. If only one or two measurements were performed in the nine-month period as per the traditional inspection interval, it would be unlikely to detect and verify the existence of any of the four irregularities. This deficiency can be largely attributed to the randomness in a single measurement run in terms of vibration, noise, and environmental interference that changes with seasons. By having more frequent inspections, the detection results can be verified by historical records, in a way that offsets the influence of randomness in each measurement. This also applies to the cases of Scale 2 and Scale 3, as the criterion for verification is essentially the same.

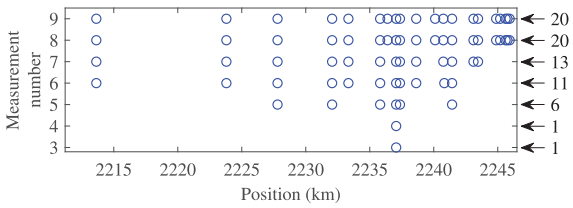

Fig. 12. Locations of verified local irregularities at Scale 2 corresponding to the number of measurements performed. Arrows on the right indicate the number of verified local irregularities (circles) accumulated after every measurement.

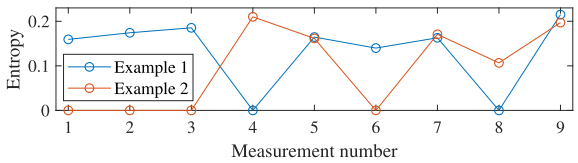

Fig. 13. Two examples of entropy evolvement at Scale 2. Example 1 shows the entropies at the position where the first and only local irregularity is verified after measurement 3. Example 2 shows the entropies at the position where the rightmost local irregularity is newly verified after measurement 8 (see Fig. 12).

2) Scale 2: The second scale is also based on the CSWs, but focus on local irregularities with a shorter length between spans and interdropper distances. The computational process is the same as in Scale 1. Fig. 12 shows the locations of verified local irregularities after a certain measurement was performed. Because it takes at least three positive results at the same location to verify a potential local irregularity identified from the first measurement (baseline), Fig. 12 presents the verified results starting from measurement 3. It can be seen that only one irregularity was verified successfully after measurements 3 and 4, which indicates that there were local irregularities left undetected in one or two of the earlier measurements. Starting from measurement 5, the number of verified local irregularities increased significantly. By the time of the sixth measurement, which was the last opportunity to verify the results from the first measurement according to (14), the number reached 11. At this point, the detection results began with measurement 1 were regarded as finalized. Thus, the newly verified irregularities after measurement 6 can be considered as the ones missing from measurement 1, or emerging ones because the railway line was still operating between the measurements. By the end of the experimental inspections, measurement 9 outputs the same number of verified local irregularities as that of measurement 8. This indicates that the inspection reached a state where the existing local irregularities were mostly verified, while the emerging ones were still labeled as potential ones from the most recent six measurements.

Fig. 13 shows the typical evolvement of entropy using two examples in Scale 2. Example 1 is a verified local

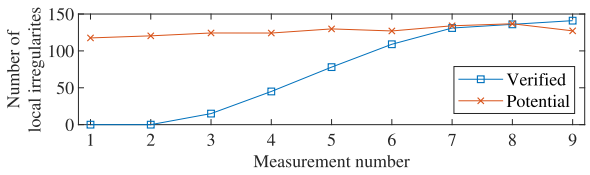

Fig. 14. Numbers of verified and potential local irregularities at Scale 3 with respect to the measurement number.

irregularity that was identified continuously in the first three measurements. This implies that the local irregularity already existed before the first measurement. However, it can be seen that measurements 4 and 8 still failed to detect it later on. On the contrary, Example 2 was verified near the end of the experimental inspections. It was missing in the first three measurements and detected initially in measurement 4. This indicates that it probably appeared later than Example 1 in the catenary. Similarly, it was also missing in later measurements 5 and 6 and then detected in measurements 7 and 8. Both the examples reflect the importance and necessity of the verifying procedure and tolerating missing detection in adjacent measurements.

3) Scale 3: This scale is based on the non-CSW signals to detect short local irregularities using the varying windows with time steps equal to the sampling interval. A single peak in the acceleration could be regarded as a local irregularity caused by the wear or a hard point of contact wire. This adds additional uncertainty to the detection results, as it is more dependent on single values of acceleration. Fig. 14 statistically shows the verified and potential local irregularities at Scale 3. Similar to Scale 2, the number of verified local irregularities increased from measurement 3 and became almost constant at measurement 9. Compared with the number of potential local irregularities identified at every measurement, it can be seen that it took six or seven measurements for the verified number to approach the potential number. Also, there were small differences between the verified number and the potential number in the latest measurements. This is because there are inevitably false positives in every measurement. Moreover, the number of verified local irregularities accumulated from measurement 1 was higher than the potential number detected from measurements 8 and 9, despite the fact that the potential number from a single measurement has increased slightly over time.

In summary, although local irregularities at the three scales induce different frequency responses in the pan-head acceleration, the same criteria proposed in the approach could still identify and verify them. The repeating entropy peaks from multiple measurements assure the existences of local irregularities and also exclude false alarms that are highly possible from a single measurement as shown by the above-mentioned results.

B. Overall Results

When comparing the results from different scales with each other, it gives insights into the temporal and spatial distributions of the detected local irregularities. These patterns

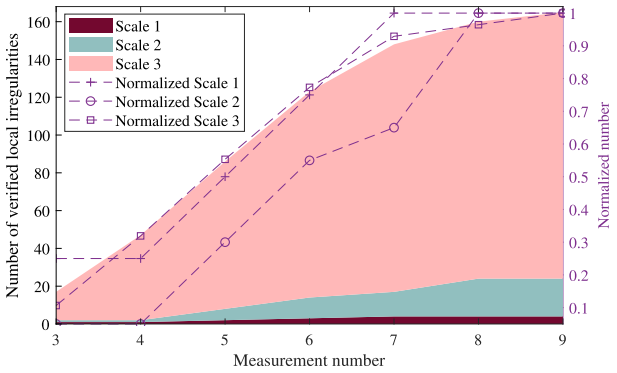

Fig. 15. Distribution and normalized numbers of verified local irregularities from the three scales with respect to the measurement number.

are important for understanding the differences among the three scales and thus treating the detection results effectively.

Fig. 15 shows the distribution of the number of verified local irregularities from the three scales. It can be seen that the total number increases rapidly starting from measurement 3 and levels off at the end of the inspections. The number from Scale 3 dominates the distribution of total number, because it has, by definition, the shortest window length to detect small defects. The tendency to grow is also mainly contributed by Scale 3, as the numbers from Scale 1 and Scale 2 became constant before measurement 9. From another perspective, the normalized numbers of every scale are shown referring to the vertical axis on the right. In this way, the slopes of the increasing numbers can be compared. From measurement 4 to 7, the slopes of the three scales are almost parallel to each other, even though the differences in number are huge. This indicates that, with the employed inspection interval, it requires about seven or eight measurements for the inspection to reach a state where most of the existing local irregularities are detected and verified. More importantly, the detection results at this point can be regarded as a new and well-established baseline, which can be utilized to reflect and distinguish the existing and emerging local irregularities. For the scale 3 specifically, one or two more measurements could help to reach this state completely.

Fig. 16(a) shows the distribution of verified local irregularities after measurement 9 by position. The positions of anchoring sections are also depicted for comparison. At Scale 1, three out of four local irregularities are located at or near the end of an anchoring section, except for the leftmost one. This indicates a high possibility of defects concerning the configuration of anchoring. At Scale 2, most local irregularities are found in the second half of the entire section, which should be paid more attention to when visiting the field. As for the ones at Scale 3, the distribution is quite dense and sporadic along the entire section. To have a closer look at the distributions, the intervals α and β marked by double-headed arrows, both containing local irregularities from the three scales, are selected. Fig. 16(b) and (c) shows the enlarged view of both the intervals. In interval α, the local irregularity at Scale 2 is located at the position of a mast, while the one in interval β is located in the middle of a span. The causes could be errors in steady arm configuration or midpoint anchor

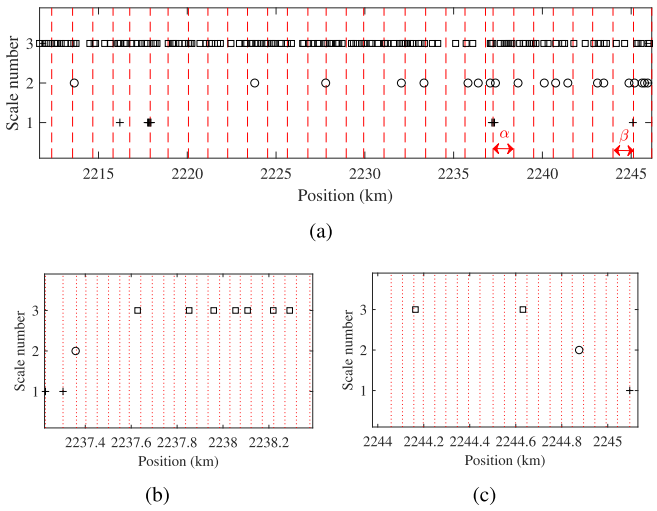

Fig. 16. (a) Positions of verified local irregularities from the three scales. The dashed lines show the positions of the ends of anchoring sections. (b) and (c) Enlarged views of the intervals α and β marked in (a), respectively. The dotted lines show the positions of masts.

misregulation. In both the intervals, the local irregularities at Scale 3 still show signs of randomness, as the defects at this scale, such as contact wire wear and hard point, can also appear at unpredictable positions.

Overall, the resulting distribution of verified local irregularities over time, as an example, shows the expected outcome from frequent inspections after a certain period of time, so that an effective schedule for further actions can be made accordingly. In the case presented, it takes approximately the first seven inspections to find most of the existing irregularities in a railway line and then set a baseline for detecting emerging irregularities in the future. Meanwhile, the distribution of local irregularities in position has certain tendencies to converge on the structural boundaries of catenary, namely the ends of spans and anchoring sections. For the verified local irregularities at Scale 1 and Scale 2, which are relatively observable and have high impacts on the pantograph–catenary interaction, it is important to set priorities for field visits depending on the density of irregularities.

V. Conclusion and Future Works

This paper proposed a new scheme for the local irregularity detection of catenary in high-speed railways based on the experimental *in situ* inspections. The inspections were carried out in a section of a high-speed line with inspection time intervals shortened from the traditional six months to an average of 39 days. This helps to explore and achieve eventually the desired inspection interval of 10 days required by the national standard [28] for high-speed railway catenaries. To achieve accurate detections, a preprocessing step is proposed for the measured pan-head accelerations. The wavelet packet entropy of the preprocessed pan-head acceleration is employed as the indicator for identifying and verifying local irregularities with different scales in length. Analyses showed that, based on the repeatability of entropies from multiple measurements, the proposed scheme can detect different scales of local irregularities that exist in a long railway line. It is simple to implement in practice while covering almost all types of local irregularities of the catenary. Furthermore, frequent inspections are beneficial to the monitoring of catenary in high-speed lines with emerging needs for condition-based maintenance. The proposed scheme is adapted and suitable for when frequent inspections are implemented in the near future.

To further develop the proposed scheme and make it feasible to cover a network of railway lines, the following can be considered.

1) The actual causes of early-stage local irregularities are not easily observable without performing additional field tests with specialized equipment. This is still an important and ongoing task to relate the detection results with actions that can be taken to facilitate maintenances.
2) Big data analytics can be applied to the massive data accumulated for long-term catenary condition monitoring.
3) The commercial trains performing the inspections and the inspection frequency should be optimized, considering the existing timetable of trains and the deterioration rate of catenary in different railway lines.

References

[1] W. Zhang, G. Mei, X. Wu, and Z. Shen, "Hybrid simulation of dynamics for the pantograph-catenary system," *Int. J. Veh. Mech. Mobility*, vol. 38, no. 6, pp. 393–414, Jun. 2002.
[2] A. Collina, F. Fossati, M. Papi, and F. Resta, "Impact of overhead line irregularity on current collection and diagnostics based on the measurement of pantograph dynamics," *Proc. Inst. Mech. Eng. F, J. Rail Rapid Transit*, vol. 221, no. 4, pp. 547–559, Jul. 2007.
[3] Z. Liu, Y. Song, Y. Han, H. Wang, J. Zhang, and Z. Han, "Advances of research on high-speed railway catenary," *J. Modern Transp.*, vol. 26, no. 1, pp. 1–23, Mar. 2018.
[4] M. Carnevale and A. Collina, "Processing of collector acceleration data for condition-based monitoring of overhead lines," *Proc. Inst. Mech. Eng. F, J. Rail Rapid Transit*, vol. 230, no. 2, pp. 472–485, Feb. 2016.
[5] H. Wang, A. Núñez, Z. Liu, Y. Song, F. Duan, and R. Dollevoet, "Analysis of the evolvement of contact wire wear irregularity in railway catenary based on historical data," *Int. J. Veh. Mech. Mobility*, vol. 56, no. 8, pp. 1207–1232, 2017.
[6] V. J. Hodge, S. O'Keefe, M. Weeks, and A. Moulds, "Wireless sensor networks for condition monitoring in the railway industry: A survey," *IEEE Trans. Intell. Transp. Syst.*, vol. 16, no. 3, pp. 1088–1106, Jun. 2015.
[7] S. Kusumi, T. Fukutani, and K. Nezu, "Diagnosis of overhead contact line based on contact force," *Quart. Rep. RTRI*, vol. 47, no. 1, pp. 39–45, 2006.
[8] M. Bocciolone, G. Bucca, A. Collina, and L. Comolli, "Pantograph–catenary monitoring by means of fibre Bragg grating sensors: Results from tests in an underground line," *Mech. Syst. Signal Process.*, vol. 41, nos. 1–2, pp. 226–238, Dec. 2013.
[9] *Railway Applications. Current Collection Systems. Requirements for and Validation of Measurements of the Dynamic Interaction between Pantograph and Overhead Contact Line*, CENELEC Standard BS EN 50317, 2012.
[10] E. Karakose, M. T. Gencoglu, M. Karakose, I. Aydin, and E. Akin, "A new experimental approach using image processing-based tracking for an efficient fault diagnosis in pantograph–catenary systems," *IEEE Trans. Ind. Informat.*, vol. 13, no. 2, pp. 635–643, Apr. 2017.
[11] P. Boffi *et al.*, "Optical fiber sensors to measure collector performance in the pantograph-catenary interaction," *IEEE Sensors J.*, vol. 9, no. 6, pp. 635–640, Jun. 2009.
[12] I. Aydin, M. Karakose, and E. Akin, "Anomaly detection using a modified kernel-based tracking in the pantograph–catenary system," *Expert Syst. Appl.*, vol. 42, no. 2, pp. 938–948, Feb. 2015.
[13] D. Zhan, D. Jing, M. Wu, D. Zhang, L. Yu, and T. Chen, "An accurate and efficient vision measurement approach for railway catenary geometry parameters," *IEEE Trans. Instrum. Meas.*, vol. 67, no. 12, pp. 2841–2853, Dec. 2018.

[14] H. Wang *et al.*, "Detection of contact wire irregularities using a quadratic time–frequency representation of the pantograph–catenary contact force," *IEEE Trans. Instrum. Meas.*, vol. 65, no. 6, pp. 1385–1397, Jun. 2016.
[15] J.-W. Kim, H.-C. Chae, B.-S. Park, S.-Y. Lee, C.-S. Han, and J.-H. Jang, "State sensitivity analysis of the pantograph system for a high-speed rail vehicle considering span length and static uplift force," *J. Sound Vib.*, vol. 303, nos. 3–5, pp. 405–427, Jun. 2007.
[16] Z. Liu, H. Wang, R. Dollevoet, Y. Song, A. Núñez, and J. Zhang, "Ensemble EMD-based automatic extraction of the catenary structure wavelength from the pantograph–catenary contact force," *IEEE Trans. Instrum. Meas.*, vol. 65, no. 10, pp. 2272–2283, Oct. 2016.
[17] D. Song, Y. Jiang, and W. Zhang, "Dynamic performance of a pantograph–catenary system with consideration of the contact surface," *Proc. Inst. Mech. Eng. F, J. Rail Rapid Transit*, vol. 232, no. 1, pp. 262–274, 2018, doi: 10.1177/0954409716664934.
[18] J. Zhang, W. Liu, and Z. Zhang, "Study on characteristics location of pantograph-catenary contact force signal based on wavelet transform," *IEEE Trans. Instrum. Meas.*, to be published, doi: 10.1109/TIM.2018.2851422.
[19] S. Mallat and W. L. Hwang, "Singularity detection and processing with wavelets," *IEEE Trans. Inf. Theory*, vol. 38, no. 2, pp. 617–643, Mar. 1992.
[20] N. E. Huang *et al.*, "The empirical mode decomposition and the Hilbert spectrum for nonlinear and non-stationary time series analysis," *Proc. Roy. Soc. A, Math. Phys. Eng. Sci.*, vol. 454, no. 1971, pp. 903–995, Mar. 1998,
[21] Z. Li, M. Molodova, A. Núñez, and R. Dollevoet, "Improvements in axle box acceleration measurements for the detection of light squats in railway infrastructure," *IEEE Trans. Ind. Electron.*, vol. 62, no. 7, pp. 4385–4397, Jul. 2015.
[22] M. Molodova, Z. Li, and A. Núñez, and R. Dollevoet, "Automatic detection of squats in railway infrastructure," *IEEE Trans. Intell. Transp. Syst.*, vol. 15, no. 5, pp. 1980–1990, Oct. 2014.
[23] S. Banerjee and M. Mitra, "Application of cross wavelet transform for ECG pattern analysis and classification," *IEEE Trans. Instrum. Meas.*, vol. 63, no. 2, pp. 326–333, Feb. 2014.
[24] E. C. C. Lau and H. Ngan, "Detection of motor bearing outer raceway defect by wavelet packet transformed motor current signature analysis," *IEEE Trans. Instrum. Meas.*, vol. 59, no. 10, pp. 2683–2690, Oct. 2010.
[25] S. Blanco, A. Figliola, R. Q. Quiroga, O. A. Rosso, and E. Serrano, "Time-frequency analysis of electroencephalogram series. III. Wavelet packets and information cost function," *Phys. Rev. E*, vol. 57, no. 1, p. 932, Jan. 1998.
[26] O. A. Rosso *et al.* "Wavelet entropy: A new tool for analysis of short duration brain electrical signals," *J. Neurosci. Methods*, vol. 105, no. 1, pp. 65–75, Jan. 2001.
[27] H. Wang, Z. Liu, A. Núñezand, and R. Dollevoet, "Identification of the catenary structure wavelength using pantograph head acceleration measurements." in *Proc. IEEE Int. Instrum. Meas. Technol. Conf.*, Turin, Italy, May 2017, pp. 1–6.
[28] *Overall Technical Specifications of Traction Power Supply Safety Inspection and Monitoring System 6C System of High-Speed Railway*, Standard 2012.136, China Railway Corporation Standard, 2012.
[29] Z. Wu and N. E. Huang, "Ensemble empirical mode decomposition: A noise-assisted data analysis method," *Adv. Adapt. Data Anal.*, vol. 1, no. 1, pp. 1–41, 2009.
[30] L. Eren and M. J. Devaney, "Bearing damage detection via wavelet packet decomposition of the stator current," *IEEE Trans. Instrum. Meas.*, vol. 53, no. 2, pp. 431–436, Apr. 2004.
[31] R. R. Coifman and M. V. Wickerhauser, "Entropy-based algorithms for best basis selection," *IEEE Trans. Inf. Theory*, vol. 38, no. 2, pp. 713–718, Mar. 1992.
[32] M. Misiti, Y. Misiti, G. Oppenheim, and J.-M. Poggi, *Wavelet Toolbox*, vol. 15. Natick, MA, USA: MathWorks, 1996, p. 21.
[33] Z. Liu, Z. Han, Y. Zhang, and Q. Zhang, "Multiwavelet packet entropy and its application in transmission line fault recognition and classification," *IEEE Trans. Neural Netw. Learn. Syst.*, vol. 25, no. 11, pp. 2043–2052, Nov. 2014.
[34] W.-X. Ren and Z.-S. Sun, "Structural damage identification by using wavelet entropy," *Eng. Struct.*, vol. 30, no. 10, pp. 2840–2849, Oct. 2008.
[35] Y. Işler and M. Kuntalp, "Combining classical HRV indices with wavelet entropy measures improves to performance in diagnosing congestive heart failure," *Comput. Biol. Med.*, vol. 37, no. 10, pp. 1502–1510, Mar. 2007.

Hongrui Wang (S'15) received the B.S. degree in electrical engineering and automation from Mao Yisheng Class, Southwest Jiaotong University, Chengdu, China, in 2012, where he is currently pursuing the Ph.D. degree with the School of Electrical Engineering.

He is also involved in a Joint Ph.D. Program with the Section of Railway Engineering, Delft University of Technology, Delft, The Netherlands. His current research interests include signal processing, machine learning, and their applications in the condition monitoring and maintenance of railway infrastructure.

Zhigang Liu (M'06–SM'16) received the Ph.D. degree in power system and automation from Southwest Jiaotong University, Chengdu, China, in 2003.

He is currently a Full Professor with the School of Electrical Engineering, Southwest Jiaotong University. His current research interests include the electrical relationship of vehicle-grid in high-speed railway, power quality considering grid-connect of new energies, pantograph-catenary dynamics, fault detection, status assessment, and active control.

Dr. Liu was elected as a fellow of The Institution of Engineering and Technology in 2017. He is an Associate Editor of the journal IEEE TRANSACTIONS ON INSTRUMENTATION AND MEASUREMENT. He is also on the Editorial Board of the journal IEEE TRANSACTIONS ON VEHICULAR TECHNOLOGY.

Alfredo Núñez (M'02–SM'14) received the Ph.D. degree in electrical engineering from the Universidad de Chile, Santiago, Chile, in 2010.

He was a Post-Doctoral Researcher with the Delft Center for Systems and Control, Delft, The Netherlands. Since 2013, he has been with the Section of Railway Engineering, Department of Engineering Structures, Faculty of Civil Engineering and Geosciences, Delft University of Technology, where he is currently an Assistant Professor (tenured) involved in data-based maintenance for railway infrastructure. He was a Work Package Leader in the development of new sensor technologies (static-, moving-, and crowd-based sensors) for railway networks in Romania, Turkey, and Slovenia, in the European Project H2020 NeTIRail-INFRA project. He has authored a book *Hybrid Predictive Control for Dynamic Transport Problems* in the Series of Advances in Industrial Control (Springer-Verlag, 2013). He has co-authored more than a hundred international journal papers and international conference papers. His current research interests include the maintenance of railway infrastructures, intelligent conditioning monitoring in railway systems, big data, risk analysis, and optimization.

Dr. Núñez is on the Editorial Board of the journal *Applied Soft Computing*.

Rolf Dollevoet received the M.Sc. degree in mechanical engineering from the Eindhoven University of Technology, Eindhoven, The Netherlands, in 2003, and the Ph.D. degree in rail research on rolling contact fatigue from the University of Twente, Enschede, The Netherlands, in 2010.

Since 2003, he has been with the Railway Sector, ProRail, Utrecht, The Netherlands. Since 2012, he has been appointed as a part-time Professor with the Section of Railway Engineering, Delft University of Technology, Delft, The Netherlands. He was also a Railway System Expert with ProRail, where he was responsible for all the scientific research and innovation with the Civil Engineering Division, ProRail Asset Management.

Dr. Dollevoet was a recipient of the Jan van Stappen Spoorprijs 2010 Award (a yearly prize for contributions to the travel quality and service for passengers in The Netherlands) from the railway sector for his Ph.D. research and its huge potential to reduce track maintenance costs.